Journal of Medicinal Chemistry

Article

Cite This: J. Med. Chem. XXXX, XXX, XXX−XXX

pubs.acs.org/jmc

Allosteric Activation of Striatal-Enriched Protein Tyrosine Phosphatase (STEP, PTPN5) by a Fragment-like Molecule

Christofer S. Tautermann,*[,†] Florian Binder,[†] Frank H. Büttner,[‡] Christian Eickmeier,[†] Dennis Fiegen,[†] Ulrike Gross,[†] Marc A. Grundl,[†] Ralf Heilker,[‡] Scott Hobson,[§] Stefan Hoerer,[†] Andreas Luippold,[‡] Volker Mack,[§] Florian Montel,[†] Stefan Peters,[†] Supriyo Bhattacharya,[∥] Nagarajan Vaidehi,[∥] Gisela Schnapp,[†] Sven Thamm,[‡] and Markus Zeeb[†]

[†]Medicinal Chemistry, [‡]Drug Discovery Sciences, and [§]CNS Diseases Research, Boehringer Ingelheim Pharma GmbH & Co KG, Birkendorfer Straße 65, D-88397 Biberach an der Riss, Germany

[∥]Department of Molecular Immunology, Beckman Research Institute of the City of Hope, 1500, E. Duarte Road, Duarte, California 91010, United States

Supporting Information

ABSTRACT: Protein tyrosine phosphatase non-receptor type 5 (PTPN5, STEP) is a brain specific phosphatase that regulates synaptic function and plasticity by modulation of *N*-methyl-D-aspartate receptor (NMDAR) and α-amino-3-hydroxy-5-methyl-4-isoxazolepropionic acid receptor (AMPAR) trafficking. Dysregulation of STEP has been linked to neurodegenerative and neuropsychiatric diseases, highlighting this enzyme as an attractive therapeutic target for drug discovery. Selective targeting of STEP with small molecules has been hampered by high conservation of the active site among protein tyrosine phosphatases. We report the discovery of the first small molecule allosteric activator for STEP that binds to the phosphatase domain. Allosteric binding is confirmed by both X-ray and ^{15}N NMR experiments, and specificity has been demonstrated by an enzymatic test cascade. Molecular dynamics simulations indicate stimulation of enzymatic activity by a long-range allosteric mechanism. To allow the scientific community to make use of this tool, we offer to provide the compound in the course of an open innovation initiative.

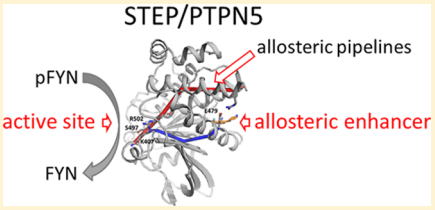

INTRODUCTION

STEP (striatal-enriched protein tyrosine phosphatase) is a critical regulator of glutamatergic synapse function and neuronal survival. STEP acts on targets directly involved in regulation of synaptic plasticity such as the NMDA and AMPA receptors, as well as several targets regulating these receptors (e.g., ERK1/2, p38, FYN, and PYK2).[1,2] Dysregulation of STEP has been attributed to the pathophysiology of various devastating neuropsychiatric disorders.[1] Whereas an upregulation of STEP has been reported in indications such as Alzheimer's disease (AD),[3] Parkinson's disease,[4] schizophrenia,[5] or fragile X syndrome,[6] a downregulation has been linked to Huntington's disease,[7,8] alcohol abuse,[9] cerebral ischemia,[10] and stress related disorders.[2] Therefore, modulation of STEP activity holds promise for the treatment of multiple CNS diseases with unmet medical need.

The efficacy of STEP modulation to alter synaptic function and affect processes of learning and memory has been indicated by genetic depletion of the enzyme[5,7] as well as pharmacologically with a moderately selective orthosteric inhibitor.[8] STEP depletion led to enhanced synaptic plasticity and rescued a behavioral phenotype in triple transgenic AD mice.[3] STEP knockout mice have been used to validate various downstream effects such as the modification of the phosphorylation state and surface expression of target NMDA[9] and AMPA[10] receptors, which have been linked to changes in synaptic plasticity such as long-term potentiation.[11] Currently, the only available pharmacological tool to modulate STEP activity is TC-2153 (**1** in Figure 1), which has been used successfully in several pharmacological studies.[8,12,13] TC-2153 is an inhibitor covalently binding to the catalytic cysteine C496, with moderate in vitro selectivity over other tyrosine phosphatases such as HePTP and PTP1B.[8] In addition a quite potent substrate derived orthosteric inhibitor has recently been reported.[14] Numerous lines of evidence suggesting that STEP

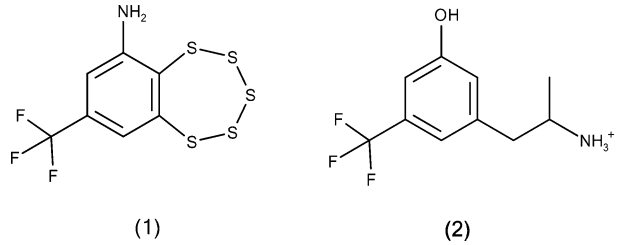

Figure 1. (**1**) Orthosterically binding STEP inhibitor TC-2153 and (**2**) the fragment screening hit binding to an allosteric pocket of the catalytic domain of STEP.

Special Issue: Allosteric Modulators

Received: May 30, 2018

DOI: 10.1021/acs.jmedchem.8b00857
J. Med. Chem. XXXX, XXX, XXX−XXX

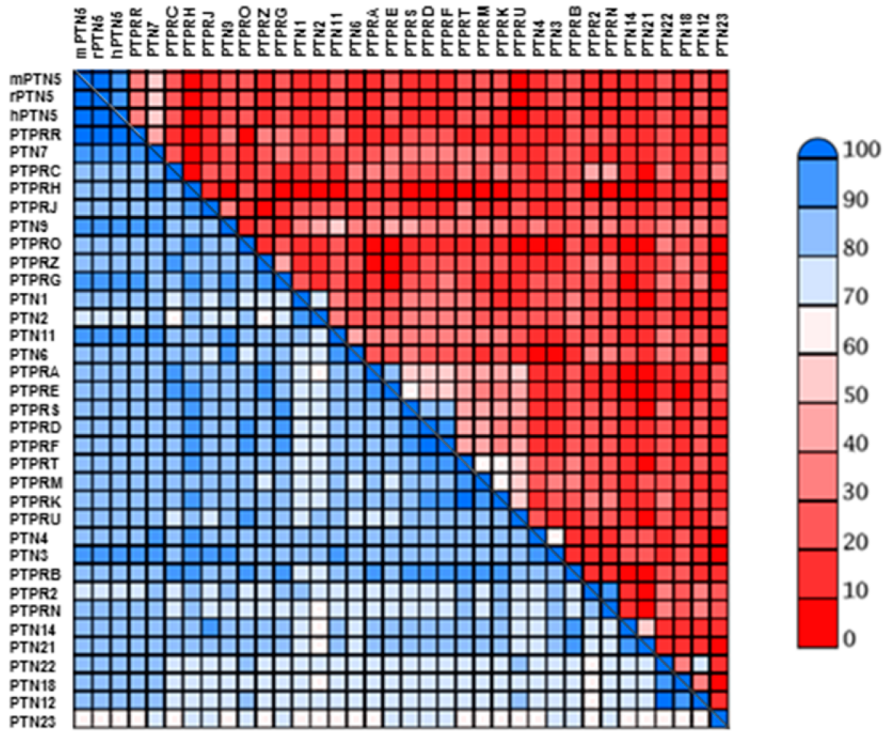

Figure 2. Sequence identities throughout the class of human PTPs. Lower triangle: sequence identity within 6 Å of the active site cysteine. Upper triangle: sequence identity within 6 Å of compound **2** bound to the allosteric site. Species conservation is displayed in the upper left 3-by-3 submatrix.

is a valuable target with the lack of selective inhibitors triggered discovery efforts toward a better starting point for STEP modulation. However, given the high polarity of the catalytic pocket and its strong structural conservation among the family of PTPs (Figure 2, lower triangle), the development of selective and potent inhibitors of PTPs is a daunting challenge. This is even more true for STEP inhibitors, for which CNS penetration is mandatory.[15] Therefore, selective tool ligands have been reported for only very few PTP family members;[16] notably to be mentioned is the recent SHP2 allosteric inhibitor by Chen et al.[17] Due to the lower conservation of remote pockets, the detection of allosterically acting ligands has been brought into focus, and for other phosphatases, such as PTP1B, allosteric inhibitors have been reported.[18,19] In the present study we describe the identification and optimization of allosteric STEP ligands that were validated as specific binders by biophysical methods. Beyond that, the most potent compound in this study (BI-0314) has been shown to act as a selective allosteric STEP activator in several biochemical assays.

RESULTS AND DISCUSSION

Detection of Allosterically Binding Fragments. STEP is a multidomain protein that exists as two splice variants, the membrane anchored longer isoform STEP61 and the cytosolic STEP46.[20] Both isoforms share the identical kinase interaction motif (KIM) and the protein tyrosine phosphatase (PTP) domain with the phosphatase consensus motif $C(X)_5R$. The KIM domain mediates binding to various target kinases with high affinity, while the PTP domain catalyzes their subsequent dephosphorylation.[21] To avoid developing ligands that potentially suffer from substrate specificity, we preferred targeting the PTP domain over the KIM domain. The PTP domain bears various conserved structural motifs, such as the WPD loop, which is crucial for the catalytic step, as its aspartate (D461) mediates proton transfer to the phosphate leaving group.[22] However, similarity analysis of the active sites of the PTP family (Figure 2, lower triangle) shows strong sequence conservation, indicating that the identification of selective active site binders will be very demanding, if not impossible. Therefore, focus was put on the identification of ligands that do not bind to the active site of STEP.

Fragment based screening has proven to be a very powerful method to detect ligands of low molecular weight binding to a target of interest.[23] A biophysical readout allows the detection of fragments binding to any site of the construct used, including allosteric pockets.[24,25] To probe for allosteric pockets on STEP, a fragment based screen was conducted on hSTEP46. A library of 3083 fragments was tested using complementary technologies, i.e., saturation transfer difference NMR (STD NMR), differential scanning fluorometry (DSF), and microscale thermophoresis (MST). The primary screen hit rate for STD NMR was very high (>15%), whereas DSF and MST yielded low hit rates (0.5% and 3%, respectively), which is indicative of hits with rather low affinity. All primary hits were subjected to 2D $^{1}H,^{15}N$ TROSY NMR, and finally, seven hits could be confirmed to bind to the PTP domain. Comparison of the chemical shift perturbation (CSP) pattern caused by the fragment hits with the ones caused by the orthosteric pan-phosphatase inhibitor Na vanadate demonstrated that an additional binding site for **2** (Figure 1) had been identified on hSTEP (Figure S1).

Following the fragment based screen, the X-ray structure of the PTP domain of hSTEP in complex with **2** was solved. The overall structure superimposes very well with published STEP structures.[22,26] Residues around the active site P- and WPD-

DOI: 10.1021/acs.jmedchem.8b00857
J. Med. Chem. XXXX, XXX, XXX−XXX

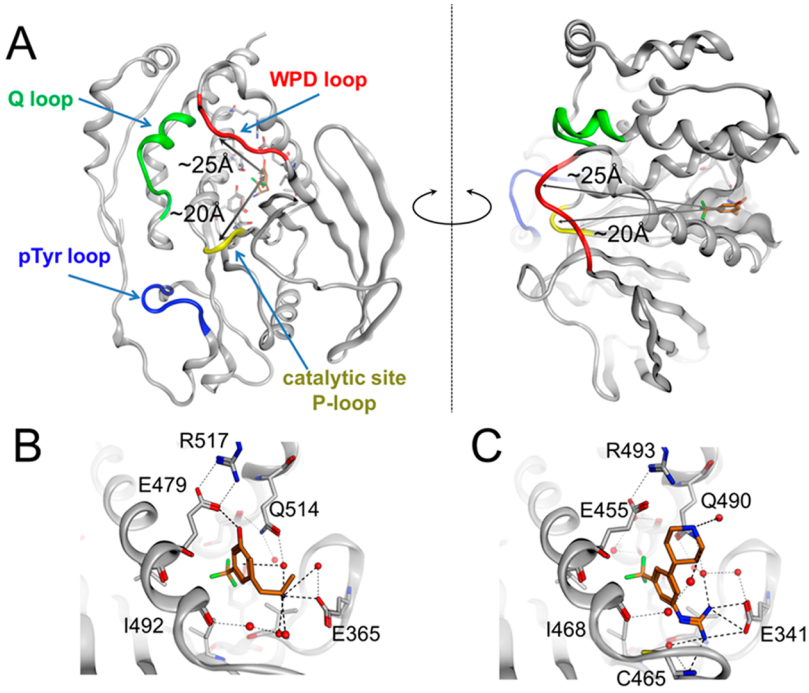

Figure 3. (A) Crystal structure of human STEP with compound **2** (orange sticks) and the distances to the active site and the WPD loop. (B) Binding mode of **2** in human STEP. (C) Binding mode of BI-0314 in murine STEP.

loops are well resolved in the electron density, while the density for the loop between β3 and β4, namely residues 400–408, is weakly defined. The active site C496 likely shows an alternative conformation and positive difference density that could be interpreted as an acetyl moiety (X-ray statistics in Table S1).

Compound **2** was found to bind to a remote pocket about 20 Å distant from the active site, on the back side of the protein (Figure 3), which will be referred to as "allosteric pocket". The sequence conservation of the allosteric pocket residues across the PTP family is very low (Figure 2, upper triangle), making this pocket ideal for the design of STEP selective ligands. Fortunately, the allosteric pocket is quite conserved within STEP orthologs (mouse, rat), reducing the risk of potential species selectivity issues. Within the allosteric pocket, compound **2** is surrounded by helices α3, α4 and the loop/3^{10}-helix between β-sheets β1 and β2 (nomenclature based on Eswaran et al.[26]). Its trifluoromethyl moiety points into a hydrophobic cleft formed by the side chains of Y369, I492, F506, and S510. The positively charged amine moiety of **2** forms a salt bridge with E365 and in addition makes water bridged contacts to C489 and Q514. The hydroxy moiety of **2** interacts with the side chain of E479 via a H-bond. In direct proximity to the binding site and the compound are residues of a symmetry related molecule (helix $\alpha2'$) that closes the pocket to the solvent (Figure S2).

As fragment growing of **2** would lead to a clash with this symmetry related molecule, a new crystal system for fragment optimization had to be established. For this purpose, murine STEP (mSTEP) was shown to be ideally suited, as a different crystal packing allowed for a fragment binding site without any close crystal contacts (Figure S2). The X-ray structure of **2** in mSTEP revealed a binding pose identical to the one in hSTEP (not shown). Importantly, specific binding of **2** to the allosteric pocket of mSTEP could also be confirmed in aqueous solution by 2D ^{15}N TROSY NMR (based on a published assignment of mSTEP,[27] Figure S1).

At this point, we had identified a new binding pocket in STEP that was also shown to be the specific ligand binding site of **2** in solution, and we had optimized the crystal system to be suitable for fragment growing by switching to a different species with a conserved allosteric binding site.

Fragment Optimization. As determined by ^{15}N NMR dose–response testing, the affinity of fragment **2** was >5 mM (data not shown). However, the fragment still showed significant shifts at 500 μM when tested by ^{15}N NMR on hSTEP (Figure S1). These results qualified ^{15}N NMR to become the driving assay for fragment optimization. Three ^{15}N NMR peaks were selected, and the cumulated H and N shifts were taken as surrogates for the changes in affinity for every compound (see Figure S1 for peak definition). The optimization of the fragments focused on the three substituents of **2** as depicted in Figure 4. The CF_3 group was found to be superior to other substituents at this position. The OH group of **2** can be exchanged by a variety of groups that occupy the crevice on the protein surface, still leading to measurable NMR shifts. Substitution by NH_2 (compound **3**) or omission (compound **4**) led to slightly weaker NMR signals compared to **2** (Table S2). The basic side chain of **2** proved to be essential for binding, which can be rationalized by the key interaction with E365. A scan of basic side chains eventually led to the discovery of **5**, revealing stronger NMR shifts compared to **4** due to additional hydrogen bonds beyond the salt bridge to E365 (Figure 3). Indeed, various other guanidine bearing analogs also displayed strong NMR shifts (data not shown). Further optimization efforts resulted in BI-0314, which was characterized by various biophysical techniques.

Crystallization trials with BI-0314 and hSTEP were not successful due to crystal contacts in the vicinity of the allosteric binding site. Nevertheless, the X-ray co-structure of BI-0314 could be determined using mSTEP (Figure 3). Confirmation

DOI: 10.1021/acs.jmedchem.8b00857
J. Med. Chem. XXXX, XXX, XXX–XXX

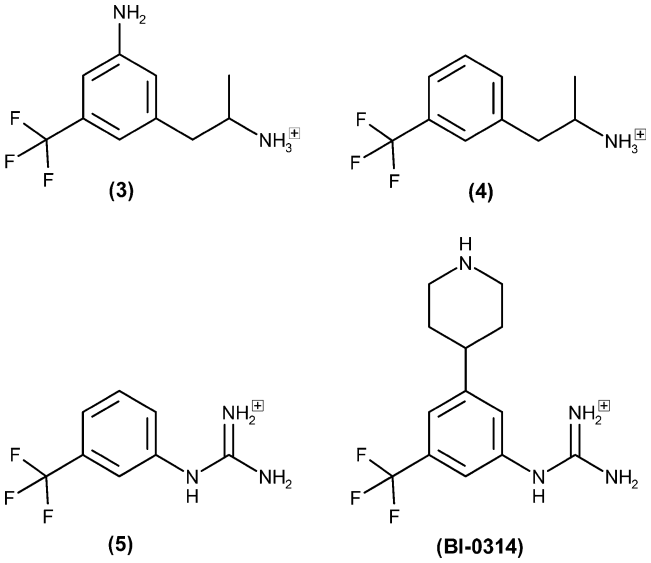

Figure 4. Snapshots of the fragment optimization of compound **2**, eventually resulting in BI-0314.

of the specificity of the binding site in solution was achieved by ^{15}N NMR on mSTEP (Figure 5, top left).[27] In analogy, very strong chemical shift perturbations are detected for human STEP in complex with BI-0314, which clearly differ from ^{15}N NMR shifts induced by the orthosteric inhibitor vanadate (Figure 5, lower panel). Furthermore, the binding affinity of BI-0314 was determined by isothermal titration calorimetry (ITC) and ^{15}N NMR on hSTEP (Figures S3 and S4). Depending on the conditions and the experimental technique, the resulting affinity was found to be 38 μM by ITC measurements (n = 3) and around 800 μM by ^{15}N NMR titration experiments. ITC experiments also revealed that binding of BI-0314 is mostly entropy driven (Figure S4).[28] To have a first estimate for selectivity on a biophysical level, binding of BI-0314 was tested on the prototypic protein phosphotyrosine phosphatase 1B (hPTP1B) by ^{15}N NMR, where no binding could be observed (data not shown).

In summary, the optimization efforts yielded the fragment like (i.e., MW < 300 Da) compound BI-0314, which is specifically binding to STEP. It has a significantly improved affinity over **2** and is selective over hPTP1B and therefore ready for characterization in functional assays.

Detection of Functional Allostery. To be close to the physiological situation, the primary enzymatic assay was performed with a phosphorylated peptide substrate derived from the endogenous substrate FYN, called pFYN-peptide. In this assay, concentration dependent amplification of hSTEP catalytic activity by BI-0314 could be observed, using both AlphaLISA and mass spectrometry (MS) as readout. The turnover of pFYN-peptide is increased by ≈30% at 100 μM and ≈60% at 500 μM. A whole set of complementary experiments was performed to demonstrate specificity of hSTEP activation (see Table 1).

Substrate dependency was tested using DiFMUP, which is a generic tool-substrate for phosphatases, changing its fluorescence when dephosphorylated.[29] Similar to the results obtained for the pFYN substrate, activation of hSTEP by BI-

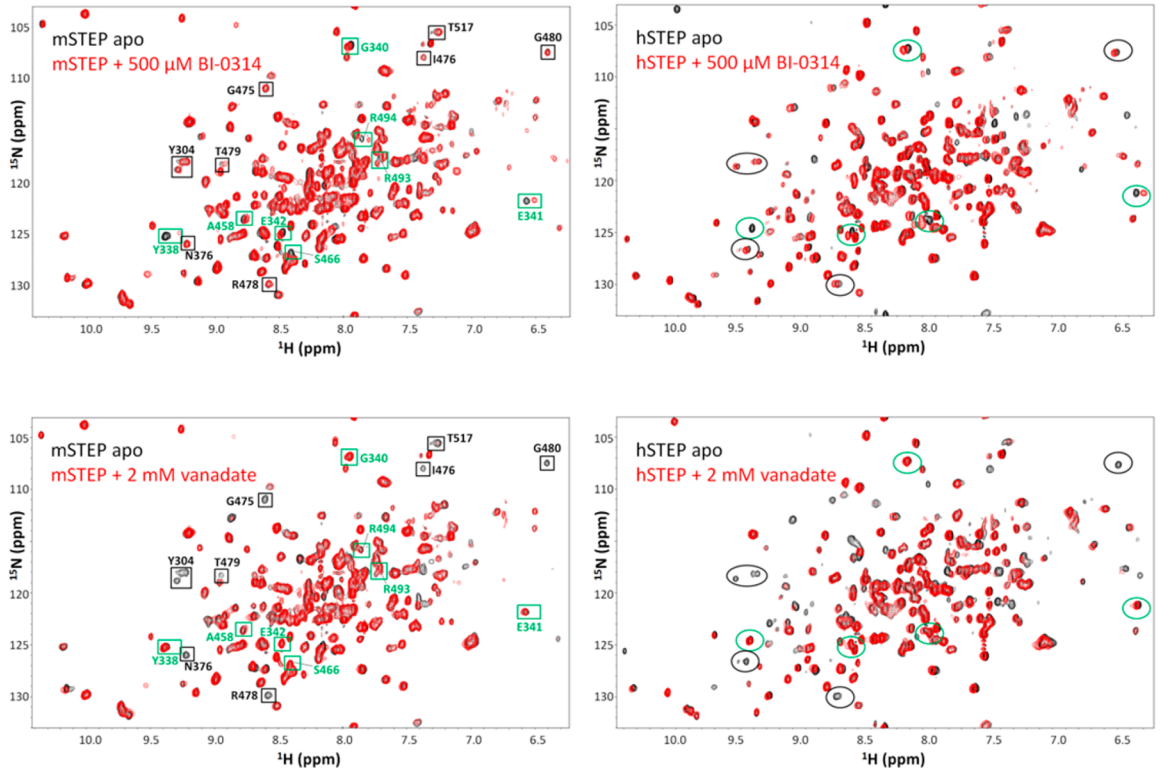

Figure 5. Superposition of 2D ^{15}N TROSY NMR spectra of 100 μM ^{2}H,^{15}N labeled human and mouse STEP PTP domain in the absence (black) or presence of BI-0314 or Na vanadate (red). Left panel: mouse STEP PTP domain in complex with 500 μM BI-0314 (top) or 2 mM Na vanadate (bottom). Cross peaks were assigned according to ref 27. Cross peaks reflecting the allosteric or orthosteric site are highlighted in green or black, respectively. Right panel: human STEP PTP domain in complex with 500 μM BI-0314 (top) or 2 mM Na vanadate (bottom). Cross peaks indicative for orthosteric (black) or allosteric (green) site binding are circled.

DOI: 10.1021/acs.jmedchem.8b00857
J. Med. Chem. XXXX, XXX, XXX−XXX

Table 1. Enzymatic Assays To Test for Specificity of STEP Activation by BI-0314

enzyme	substrate	assay technology	effect of BI-0314 in assay	learning
hSTEP46	pFYN-peptide	AlphaLISA	Activating, 56% ± 5% at 500 μM (n = 8), 33% ± 12% at 100 μM (n = 12)	BI-0314 has an activating effect on hSTEP dephosphorylation capability on pFYN-peptide.
hSTEP46	pFYN-peptide	RapidFire (MS)	Activating, 28% ± 5% at 100 μM (n = 4)	Activating effect is assay technology independent.
PTP domain of hSTEP	pFYN-peptide	AlphaLISA	Activating, 61% ± 6% at 500 μM (n = 10)	Activation also observed on the PTP domain itself.
hSTEP46	DiFMUP	Fluorescence	Activating, 48% ± 8% at 1000 μM (n = 3), 27% ± 5% at 300 μM (n = 3)	Activating effect is also observed for another substrate and different assay readout.
hPTP1B	Insulin receptor peptide	AlphaScreen	No effect at 500 μM (n = 2)	Selectivity over hPTP1B
hTCPTP	Insulin receptor peptide	AlphaScreen	No effect at 500 μM (n = 2)	Selectivity over hTCPTP
hPTP1B	pFYN-peptide	AlphaScreen	No effect at 500 μM (n = 2)	Activation effect is not pFYN peptide mediated.

Table 2. Michaelis–Menten Parameter Values for the Dephosphorylation of pFYN-Peptide by hSTEP PTP Domain with and without BI-0314

	n	K_M [μM]	k_{cat} [s^{-1}]	k_{cat}/K_M [M^{-1} s^{-1}]
hSTEP + pFYN-peptide	4	60.8 ± 7.9	0.024 ± 0.002	400 ± 20
BI-0314 + hSTEP + pFYN-peptide	8	65.4 ± 13.9	0.042 ± 0.005	650 ± 50

0314 could also be demonstrated using DiFMUP. AlphaScreen assays were performed on the closely related phosphatases hPTP1B and hTCPTP with an insulin receptor derived peptide to demonstrate selectivity. BI-0314 was inactive on both targets. Additionally, BI-0314 did not enhance the dephosphorylation of the pFYN-peptide by hPTP1B, which again confirms a hSTEP dependent mechanism rather than a substrate specific effect. To narrow down the structural basis of action of BI-0314, we also demonstrated activation in an assay with the PTP domain of hSTEP. A trend toward activation can also be demonstrated on mouse STEP PTP domain (Figure S5), but the effect is smaller than on human STEP.

In order to gain insight into the mechanism of action of BI-0314 on hSTEP, we derived Michaelis–Menten parameters for the hSTEP/pFYN-peptide system in the absence or presence of 500 μM BI-0314 employing the PTP domain of hSTEP and RapidFire readout (Table 2 and Figure S6). Determined values for K_M are well in line with values reported by Li et al.;[21] however k_{cat} is somewhat lower than reported.[21] These differences may arise from different assay conditions employed. Addition of BI-0314 caused an acceleration of the enzymatic reaction catalyzed by hSTEP, which is reflected in an increase of k_{cat} while keeping the K_M for the pFYN-peptide unchanged. Mechanistically this implies that binding of BI-0314 to the allosteric site causes a higher turnover of the pFYN-peptide without changing the affinity of this substrate for hSTEP. Therefore, the k_{cat}/K_M ratio, which is a measure for the catalytic efficiency, is significantly increased by BI-0314. In analogy to allosteric noncompetitive inhibition, where the catalytic efficiency is decreased by a reduced k_{cat} with a constant K_M, we identify BI-0314 as an allosteric activator of hSTEP.

Mechanism of Allostery. To investigate the molecular mechanism of communication between the allosteric binding site and the active site, we calculated the allosteric communication pipelines in STEP using the Allosteer method (Figure S7).[30] This method relies on a graph theory algorithm combined with the mutual information in torsion angles between residue pairs and has been successfully validated to study long-range communication in G-protein-coupled receptors.[30] Two of the strongest pipelines emerging from the active site connect to the allosteric binding site of BI-0314, as shown in Figure 6. On the basis of the mutual information

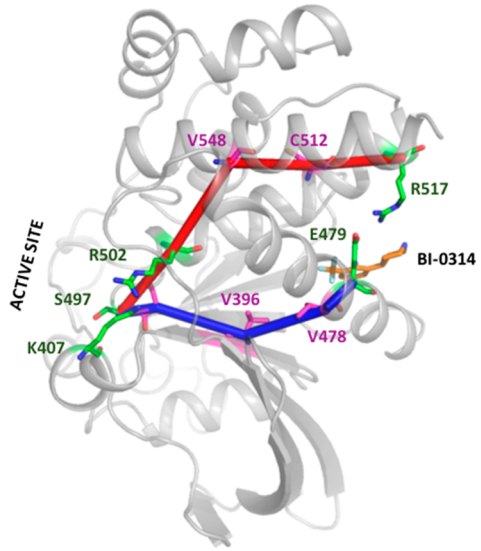

Figure 6. Allosteric pipelines in hSTEP communicating between the active site and the BI-0314 binding site displaying the allosterically active residues in both pockets (green residues). Important allosteric hub residues along the communication pipelines are shown in magenta.

analysis, residues K407, S497, and R502 in the active site show highly correlated motion with the allosteric site. Specifically, S497, which is neighboring the catalytic C496, is known to be involved in the pTyr dephosphorylation mechanism.[31] On the other hand, looking at the allosteric site, the residues R517 and E479 show strong allosteric communication with the active site. These two residues form a salt bridge and also make close contacts with BI-0314. We speculate that the interaction of BI-0314 with this salt bridge mediates the allosteric communication with the active site and thereby stabilizes the active conformation of STEP. Comparison of apo and ligand bound

DOI: 10.1021/acs.jmedchem.8b00857
J. Med. Chem. XXXX, XXX, XXX–XXX

Scheme 1. Synthesis of BI-0314[a]

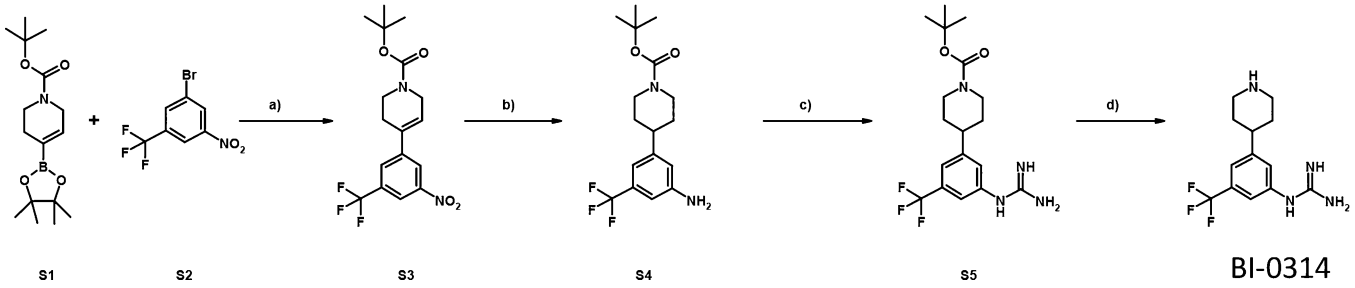

[a]Reagents and conditions: (a) Cs_2CO_3, Pd(dppf)Cl_2, dioxane, 100 °C, 82%; (b) RaNi, H_2, EtOAc, EtOH, 50 °C, 78%; (c) $NH_2C(=NH)SO_2H$, MeOH, 100 °C, 13%; (d) TFA, DCM, rt, 22%.

structures of mSTEP confirms a change in conformation of the salt bridge (Figure S8) and therefore strengthens our hypothesis. Further support is coming from a comparison of residues significantly contributing to allosteric communication (allosteric hubs in Figure 6) to the corresponding residues in PTP1B (Figure S11). Upon ligand binding the flexibility of these residues in PTP1B is altered,[32,33] experimentally demonstrating the allosteric communication along these pathways.

When corroborating these results with extensive plain MD simulations, we observe a strong impact on the WPD loop. Upon binding of BI-0314, the flexibility of the WPD loop decreases (Figure S9), again proving the long-range allosteric action extending more than 20 Å across the PTP domain. This decrease in flexibility and increase in stabilizing interactions could be confirmed experimentally using differential scanning fluorometry. Heat induced unfolding of hSTEP revealed an elevated melting temperature in the presence of 500 μM BI-0314 (T_m shift of 1.4 °C (n = 7)), whereas for **2** no stabilization of the native conformation could be detected (Figure S10).

Taking these results together, we are confident that the two pockets are connected by allosteric communication and hypothesize that binding of BI-0314 employs this mechanism to impact the catalytic efficiency of STEP.

CONCLUSIONS

BI-0314 is the first allosteric ligand reported for hSTEP, which is a highly interesting target to potentially treat various psychiatric conditions as well as neurodegenerative diseases. The allosteric binding pocket on STEP was identified by a fragment-based screen, where one very weakly binding primary hit was optimized, yielding a compound with sufficient binding affinity to allow testing in biochemical assays. To rule out that the observed effects were assay or substrate specific artifacts, a set of experiments assessing different substrates, other phosphatases, and different assay technologies were performed. BI-0314 is a hSTEP specific positive allosteric modulator and has been shown to be inactive on two other related tyrosine phosphatases due to the low conservation of the residues in the allosteric site. Derivation of the Michaelis–Menten parameters of hSTEP mediated dephosphorylation reaction of pFYN-peptide in the presence or absence of BI-0314 showed that the ligand causes an increase in k_{cat} leading to an enhanced turnover rate. On the basis of MD simulations, the mechanism can be explained by a long-range interaction via allosteric communication between the allosteric binding site and the active site, where BI-0314 binding results in a significant change in the flexibility of the catalytically important WPD loop.

The discovery of a functionally active allosteric binding site on STEP is another example demonstrating that fragment-based drug discovery is a very powerful method to identify chemical tools after limited cycles of optimization. As shown by many groups, the discovery of STEP selective ligands is a challenging task when employing classical high throughput screening approaches.[8] Until now, no selective small molecule activator of STEP has been reported. Therefore, the discovery of an allosteric site on STEP that is amenable to designing selective modulators of its catalytic activity represents a breakthrough to successfully targeting STEP. However, to transform BI-0314 into a ligand that is suitable for in vivo testing, further optimization or specifically screening for ligands binding to the reported allosteric site will be required. Upon having demonstrated hSTEP activation by BI-0314, no further optimization on ligands targeting this allosteric site was performed, since we originally had set out to identify STEP inhibitors. The discovery of BI-0314 and its allosteric site demonstrates that phosphatases are indeed druggable but will require new and smart approaches to identify selective ligands that have the potential to become drugs.

The disclosure of BI-0314 should spark research in the direction of developing allosteric enhancers of phosphatases. Therefore, we offer to share BI-0314 in the course of an open innovation initiative (https://opnme.com/) where the compound can be obtained by research groups free of charge.

EXPERIMENTAL SECTION

Compound Purity. Compounds **2**, **3**, **4**, **5**, and BI-0314 have been determined to be >95% pure by HPLC/MS.

Compound Synthesis. Compounds **2**–**5** are commercially available.

Synthesis of BI-0314. The synthesis of BI-0314 is shown in Scheme 1 and is described below.

Tert-butyl 4-[3-nitro-5-(trifluoromethyl)phenyl]- 1,2,3,6-tetrahydropyridine-1-carboxylate (S3). 3-Bromo-5-nitrobenzotrifluoride (**S2**) (405 mg, 1.50 mmol) and boronic ester **S1** (557 mg, 1.80 mmol, 1.2 equiv) were dissolved in dioxane (18 mL). The solution was degassed with argon. An aqueous solution of Cs_2CO_3 (2 M, 3 mL, 6 mmol, 4 equiv) was added, and the reaction mixture was degassed with argon. The reaction mixture was heated to 100 °C overnight. It was poured into water (60 mL) and was extracted with $CHCl_3$ (2 × 30 mL). The combined extracts were washed with aqueous solution of HCl (0.1 M, 2 × 30 mL) and brine (1 × 30 mL) and were filtered through a plug of Celite and then through a plug of Alox. The filtrate was evaporated in vacuo to yield the desired product **S3** (542 mg, 85% purity by HPLC, 1.24 mmol, 83%). HPLC–MS (method A): t_R = 1.28 min. MS: $(M + H - CH_2C(CH_3)_2)^+$ 317.

DOI: 10.1021/acs.jmedchem.8b00857
J. Med. Chem. XXXX, XXX, XXX–XXX

Tert-butyl 4-[3-amino-5- (trifluoromethyl)phenyl]-piperidine-1-carboxylate (S4). **S3** (542 mg, 85% purity, 1.24 mmol) was dissolved in EtOAc (15 mL) and EtOH (15 mL). RaNi (500 mg, 8.52 mmol, 7 equiv) and H_2 (50 bar) were added. The reaction was stirred at 50 °C for 1 d. The catalyst was removed by filtration. The filtrate was evaporated in vacuo. The crude product was purified by preperative HPLC to yield the desired product **S4** (332 mg, 0.964 mmol, 78%). HPLC−MS (method A): t_R = 1.14 min. MS: $(M + H - CH_2C(CH_3)_2)^+$ 289.

Tert-butyl 4-[3-carbamimidamido-5- (trifluoromethyl)-phenyl]piperidine-1-carboxylate (S5). **S4** (200 mg, 0.581 mmol) and formamidine sulfinic acid (144 mg, 1.16 mmol, 2.0 equiv) were dissolved in degassed MeOH (4 mL). The reaction mixture was stirred at 100 °C for 3 d. ACN and water were added and the mixture was purified by preparative HPLC to yield the desired product (29 mg, 0.075 mmol, 13%). HPLC−MS (method A): t_R = 0,94 min. MS: $(M + H)^+$ 387.

N-[3-(piperidin-4-yl)-5- (trifluoromethyl)phenyl]guanidine (BI-0314). **S5** (29 mg, 0.075 mmol) was dissolved in DCM (1 mL). TFA (95%, 1 mL) was added at rt. After 2 h the mixture was evaporated to dryness. The residue was dissolved in an ACN/water mixture and was purified by preparative HPLC to yield the desired product BI-0314 as double TFA salt (8.0 mg, 0.016 mmol, 22%). HPLC−MS (method A): t_R = 0.63 min. MS: $(M + H)^+$ 287. ^{1}H NMR (400 MHz, DMSO-d_6) δ 10.15 (s, 1H), 8.70 (br s, 1H), 8.42 (br s, 1H), 7.74 (s, 4H), 7.44−7.47 (m, 2H), 7.38 (dd, J = 1.0 Hz, 1H), 3.40 (d, J = 1.0 Hz, 2H), 2.94−3.06 (m, 3H), 1.99 (br d, J = 13.2 Hz, 2H), 1.81 (qd, J = 13.1, 4.0 Hz, 2H).

Analytical Methods. NMR spectra were recorded on a Bruker 400 MHz instrument. Chemical shifts are given in parts per million (ppm) downfield from internal reference tetramethylsilane in δ units. Selected data are reported in the following manner: chemical shift, multiplicity (s = singlet, d = doublet, dd = double doublet, t = triplet, q = quartet, m = multiplet), coupling constants (J), integration.

Mass spectra were obtained using a liquid chromatography mass spectrometer (HPLC−MS) that consisted of Agilent 1200 LC with DA- and MS-detector.

Retention times (t_R) were obtained using Agilent 1200 liquid chromatography−mass spectrometer (HPLC−MS), using the following method shown in Table 3.

Table 3. HPLC−MS Method A[a]

	gradient/solvent			
time [min]	% sol [H_2O, 0.1 % TFA]	% sol [ACN]	flow [mL/min]	temp [°C]
0	97	3	2.2	60
0.2	97	3	2.2	60
1.2	0	100	2.2	60
1.25	0	100	3	60
1.4	0	100	3	60

[a]Column: Sunfire C18, 3.0 mm × 30 mm, 2.5 μm. Column supplier: Waters.

NMR Spectroscopy. STD-NMR experiments experiments[34] were carried out on a Bruker Avance II 600 MHz instrument equipped with a QCI cryogenic probe and z-gradients. Selective irridation for 3 s was achieved with a Gaussian pulse train at −0.2 ppm for the on-resonance and 60 ppm for the off-resonance spectrum. A 30 ms spin-lock pulse was used to suppress protein signals, and both spectra were subtracted after acquisition to yield the difference spectrum. Fragments were tested in mixtures of four compounds (each at 250 μM) in 20 mM Tris-d11, 100 mM NaCl, 1 mM TCEP, pH 7.4, in D_2O in the presence of 4 μM STEP46. Signals in the difference spectrum are indicative for binding, and hits were identified by comparing to individual prerecorded reference spectra. The entire fragment library was characterized with respect to purity, identity, buffer solubility, and self-STD effects. Samples were freshly prepared just in time with an in-house customized Tecan Freedom Evo liquid handler[35] to achieve NMR sample tube filling. Transfer of the samples (140 μL in 2.5 mm NMR tubes) to the magnet was accomplished with the Bruker Sample Rail system. Fragments were either purchased from various external vendors or selected from internal proprietary sources.

Confirmation of primary FBS hits obtained from STD-NMR, DSF, and MST were performed using two-dimensional ^{1}H,^{15}N TROSY NMR spectra[36] collected on a Bruker Avance III 600 MHz spectrometer equipped with a 5 mm z-gradient TCI cryoprobe and a Bruker Sample Rail. Each sample contained 40 μM ^{15}N labeled STEP PTP in 20 mM Tris-d11, 100 mM NaCl, 1 mM TCEP, pH 7.4, and 8% (v/v) D_2O. The protein was incubated with 500 μM fragment in a 2.5 mm NMR tube at 298 K and a DMSO-d_6 concentration of 1%. Spectra were recorded with 192 transients and 64 data points in the indirect dimension. Processing and analysis were done with the Topspin 3.0 software (Bruker BioSpin). Binders were identified by manual comparison of spectra in the presence of a fragment and the STEP PTP reference spectrum.

Differential Scanning Fluorimetry (DSF). DSF experiments were carried out in a Bio-Rad CFX384 real-time system (C1000Touch Thermal Cycler) in sealed Hard-Shell PCR 384-well plates (no. HSP3805; PCR Sealers; no. MSB1001; Bio-Rad) and a total volume of 10 μL. The assay was optimized regarding protein consumption and SYPRO Orange dye excess (5000× concentration in DMSO, Invitrogen) to obtain a reliable fluorescence signal. Compound dilutions in assay buffer (20 mM HEPES, pH 7.5; 50 mM NaCl; 1 mM TCEP) were prepared as duplicates by a Hamilton Microlab Starlet pipetting robot, whereas the protein/dye stock solution was added manually with a multichannel pipet. The reaction mixture contained 8 μL compound dilution and 2 μL of the STEP46 SYPRO Orange stock mix to yield final concentrations of 5 μM STEP46, 25× SYPRO Orange and 500 μM fragment (1% DMSO). Samples were heated at 1 °C/min from 25 to 95 °C with fluorescence readings every 0.5 °C. Melting curves were analyzed with the Bio-Rad CFX Manager data analysis software by plotting the first derivative of the recorded fluorescence intensity versus the temperature where the minimum of such a curve corresponds to the T_m value. Thermal shifts of $\Delta T_m \geq 0.5$ °C ($\Delta T_m = T_{m,frag} - T_{m,DMSO}$) were assumed significant and defined as primary FBS hits.

Xray. Protein crystallization was done using the hanging drop method by mixing 1 μL of hSTEP complexed with 5 mM compound **2** (from a 100 mM DMSO stock solution) with 1 μL of reservoir solution (24% PEG 3350, 0.2 M ammonium sulfate, and 0.1 M Bis-Tris, pH 5.5) at 4 °C. Crystals were flash frozen in liquid nitrogen. Crystallization of mSTEP was also done via the hanging drop method at 4 °C in a 24-well plate. The reservoir solution contained 26% PEG 3350, 0.1 M Tris, pH 7.8, 0.2 M ammonium citrate. For the drops 1 μL of apo protein was mixed with 1 μL of the reservoir. First crystals appeared after 8 days. Apo crystals were transferred to a soaking and cryo buffer containing 25% PEG3350, 0.2 M Bis-Tris, pH 7.5, 0.2 M disodium malonate and soaked for 4 h in the presence of 100 mM BI-0314. Crystals were flash frozen in liquid nitrogen, and data were collected at the SLS beamline X06DA (Swiss Light Source, Paul Scherrer Institute) at a wavelength of 1 Å using the PILATUS 2M detector. The crystals belonged to space group P212121 (hSTEP) or P41212 (mSTEP) and contained one monomer per asymmetric unit. Images were processed with autoPROC.[37] The resolution limits were set using default autoPROC settings. The structures were solved by molecular replacement using the STEP structure 2BIJ[26] as a search model. Subsequent model building and refinement was done using standard protocols using CCP4,[38] COOT[39] and autoBUSTER.[40]

The unit cell parameters of the hSTEP−compound **2** complex were a = 53.1 Å, b = 64.4 Å, c = 100.8 Å and α, β, γ = 90°, and the structure was refined to R_{work} and R_{free} values of 20.0% and 23.9%, respectively, with 95% of the residues in Ramachandran favored regions as validated with Molprobity.[41] The unit cell parameters of the mSTEP−compound BI-0314 were a = 59.3 Å, b = 59.3 Å, c = 181.6 Å, α, β, γ = 90° and was refined to R/R_{free} = 18.1/21.2% with 95% of the residues in Ramachandran favored regions.

DOI: 10.1021/acs.jmedchem.8b00857
J. Med. Chem. XXXX, XXX, XXX−XXX

ITC (Isothermal Titration Calorimetry) Analysis. Experiments using isothermal titration calorimetry were conducted on a MicroCal auto iTC200 instrument with hSTEP PTP domain that had been passed through a PD-10 desalting column (GE Healthcare) equilibrated with 10 mM HEPES, 200 mM NaCl, and 0.5 mM TCEP, pH 7.5. Complete saturation of 200 μM of hSTEP was typically achieved by injecting 18 × 2 μL aliquots of 2 mM BI-0314 at 25 °C. The thermodynamic binding parameters were extracted by nonlinear regression analysis of the binding isotherms (MicroCal Origin software, version 7.0). A single-site binding model was applied yielding the binding enthalpy (ΔH), stoichiometry (n), entropy (ΔS), and association constant (K_a). Data are mean values from three independent titrations with calculated standard deviation.

Protein Expression and Purification. The gene corresponding to amino acid residues 197−565 (STEP46) or 281−563 (STEP PTP domain) of human STEP (PTN5 human, Uniprot code P54829) was produced by gene synthesis (optimized for *E. coli* expression) with an N-terminal 6 His-tag followed by a TEV protease site and cloned into pET24a (Novagen) with NdeI and *Eco*RI. The gene corresponding to amino acid residues 244−539 of mouse STEP (PTN5 mouse, Uniprot code P54830) was synthesized and cloned identical to human STEP.

The expression plasmids for STEP proteins were transformed in BL21 (DE3) cells (Novagen), and cells were grown in LB containing 30 μM kanamycin at 37 °C to mid log phase, and protein expression was induced with 1 mM IPTG. The temperature was then reduced, and cells were grown for further 16 h at 18 °C. Cells were harvested, resuspended in lysis buffer (50 mM HEPES, 500 mM NaCl, 0.5 mM TCEP, and protease inhibitors (complete EDTA free, Roche Diagnostics), pH 7.5, and lysed by the Constant Cell Disruption System. The fusion protein was purified using Ni-NTA (Qiagen) affinity and eluted with buffer containing 250 mM imidazole. STEP protein was further purified by gel filtration using Superdex 200 HR column (GE Healthcare) equilibrated in 10 mM HEPES, pH 7.5, 200 mM NaCl, and 0.5 mM TCEP. The protein was concentrated to 10 mg/mL for crystallization and to 5 mg/mL for NMR studies. For ^{15}N or ^{2}H,^{15}N labeling STEP was expressed in Silantes *E. coli* OD2 N, ^{15}N medium or in Silantes *E. coli* OD2 DN, ^{2}H, ^{15}N medium, respectively.

STEP-pFYN-peptide AlphaLISA Assay. Compounds are serial diluted in 100% DMSO in a 384-well PP microplate V-shape (Greiner no. 781280) using an Agilent Bravo pipetting robot. With an intermediate dilution step in AlphaLISA assay buffer (PerkinElmer no. AL000F) in a 384-well clear PS microplate (Greiner no. 781101), the DMSO concentration is reduced to achieve 1% DMSO in the final assay reaction. The assay in a 384-well Optiplate (PerkinElmer no. 6007290) starts by addition of 5 μL of diluted compound, 5 μL of STEP46 (50 nM f.c.; 46 kDa fragment of STEP (STEP46) produced in the laboratory of Dr. Gisela Schnapp, Boehringer Ingelheim Pharma GmbH & Co. KG) and 5 μL pFyn peptide (20 nM f.c.; (biotin-GLARLIEDNE-Y(H2PO3)-TARQGAKFPI-OH), purity >95%, custom synthesized, and purchased via Biotrend), followed by short centrifugation. The assay mixture is incubated at room temperature for 60 min in the dark. After incubation, 5 μL/well of anti non-phospho Src/Tyr416 antibody (Cell Signaling Technology no. 2102), diluted in enzyme stop buffer (AlphaLISA ImmunoAssay buffer, supplemented with 10 μM sodium orthovanadate) is added to each well (final antibody dilution 1:26 000 in 15 μL of detection volume). Next, 5 μL/well of protein A-coated ALPHA acceptor beads (PerkinElmer no. 6760617M) in enzyme stop buffer is added to each well. The assay mixture is incubated for 15 min at room temperature covered with a plate lid. After incubation, 5 μL/well of streptavidin-coated ALPHA donor beads in enzyme stop buffer is added to each well. The assay mixture is incubated for 15 min at room temperature with a plate lid. Finally, the signal is measured using an Envision reader (PerkinElmer). Each assay plate contains wells with "high" and "low" controls, where "high" controls (100% CTL) are defined as 50 nM STEP46 incubated with 20 nM pFyn peptide and "low" controls (0% CTL) are defined as 20 nM pFyn peptide without STEP46. The "percent control" (% CTL) values are calculated as follows: % CTL = 100 × (AlphaLISA (sample) − AlphaLISA ("low" control))/(AlphaLISA ("high" control) − AlphaLISA ("low" control)). Optimized assay conditions for the AlphaLISA assay on hSTEP PTP domain were as above but with 20 nM hSTEP PTP and 3 nM pFYN peptide.

STEP-RapidFire MS/MS Assay. Nonbiotinylated Fyn-peptide (BioTrend no. 435305) is diluted in assay buffer (1 M HEPES, Invitrogen no. 15630-056 (50 mM f.c.); Brij35, Roth no. CN21.1 (0.02% f.c), DTT, Sigma no. D5545 (1 mM f.c.). In a 384-well Optiplate (PerkinElmer no. 6007290), 5 μL/well of the diluted substrate, 5 μL/well of STEP46 (50 nM f.c.; 46 kDa fragment of STEP (STEP46) produced in the laboratory of Dr. Gisela Schnapp, Boehringer Ingelheim Pharma GmbH & Co. KG) and 5 μL/well of prediluted compound (500 μM f.c.) are mixed and incubated for 1 h at room temperature. The reaction was stopped by adding 5 μL/well of a sodium orthovanadate solution (12 μM f.c.). An amount of 15 μL of the stopped enzymatic reaction is transferred to a 384-well polypropylene microplate (Masterblock 22 mm; Greiner no. 781280) and mixed with 135 μL of Fyn labeled internal standard solution (GLA[R(13C6; 15N4)]LIEDNEYTARQGAKFPI), Thermo Fisher). The analytical sample handling was performed by a rapid-injecting RapidFire autosampler system (Agilent, Waldbronn, Germany) coupled to a triple quadrupole mass spectrometer (TSQ Vantage, ThermoFisher, San Jose, CA, USA). Liquid sample is aspirated by a vacuum pump into a 10 μL sample loop for 250 ms and subsequently flushed for 3000 ms onto a C18 cartridge (Agilent, Waldbronn, Germany) with the aqueous mobile phase (99.5% water, 0.5% acetic acid, flow rate 1.5 mL/min). The solid phase extraction step retains the analyte while removing interfering matrix (e.g., buffer components). The analyte is desorbed and back-eluted from the cartridge for 3000 ms with an organic mobile phase (99.5% methanol, 0.5% acetic acid, flow rate 1.25 mL/min) and flushed into the mass spectrometer for detection in MRM mode. The MRM transition for the FYN peptide is 788.48 < 994.27 Da (S-lense 156 V, collision energy 28 V) and for the internal standard 791.66 < 1073.18 Da (S-lense 200 V, collision energy 22 V). Dwell time for each MRM transition is 25 ms, and pause time between MRMs is 5 ms. The mass spectrometer is equipped with the HESI II ion source and operated in positive ionization mode (ion spray voltage 2500 V, capillary temp 325 °C, sheath gas pressure 30 Au, vaporizer temp 500 °C, aux gas pressure 45 Au). While performing the back flush into the mass spectrometer, the sample loop and relevant tubing were flushed with the organic mobile phase to prevent carryover of analyte or matrix components into the next sample. Equilibration time for the system is 500 ms. In order to further minimize carryover effects, the wash station of the RapidFire system was used to perform needle washes with pure water (100%) and pure methanol (100%) between samples. The solvent delivery setup of the RapidFire system consists of three continuously running and isocratically operating HPLC pumps (G1310A, Agilent, Waldbronn, Germany). MS data processing was performed in GMSU (Alpharetta, GA, USA), and peak area ratio FYN peptide/internal standard was reported for IC_{50} calculation.

STEP-DiFMUP Assay. Buffer for the DiFMUP assay was the same as listed previously. DiFMUP (Life Tech no. D6567) stock solutions were prepared at 10 mM in DMSO and stored at −20 °C. Test compounds were received as 50 mM stock solutions in DMSO and stored at −20 °C. Purified human STEP46 was the same as previously listed.

Compounds were diluted to 20× final test concentration in DMSO. An amount of 2.5 μL was then pipetted into a 384-well black, flat-bottom assay plate (Corning no. 3573). Purified human STEP46 was prediluted in ice cold assay buffer to 210 nM, after which an amount of 23.5 μL was added to the assay plate and incubated for 10 min at room temperature. DiFMUP substrate was diluted with buffer to 2 μM, after which the assay was initiated by adding 24 μL to the assay plate, giving final reaction conditions of 50 mM HEPES, 0.02% Brij 35, 1 mM DTT, 1 μM DiFMUP, 100 nM STEP46, and 5% DMSO. Fluorescence intensity (excitation 340 nm; emission 460 nm) was monitored in a Fluoroskan Ascent (PerkinElmer) at 1 min intervals for 30 min at 37 °C. Background signal, determined by not adding STEP46 enzyme, was subtracted from assay signals. The linear signal

DOI: 10.1021/acs.jmedchem.8b00857
J. Med. Chem. XXXX, XXX, XXX−XXX

increase (Δsignal increase/min) for STEP46 in the absence of compound or at different compound concentrations was calculated, and STEP46 in the absence of compound was set to 100%.

PTP1B, TC-PTP-insulin Receptor Derived Substrate and PTP1B pFYN Substrate Assays. For all phosphatase assays the AlphaScreen technology was employed. Assays were set up as competition assays generating a high assay signal using biotin-Ahx-EDT-pY-Y-RKG-amide and anti-phosphotyrosine antibody 4G10. Unbiotinylated substrate is competing with the antibody binding and therefore reducing the AlphaScreen signal. For every phosphatase assay white 384-well microplates Lumitrac 200 (Greiner, Friggenhausen, Germany, catalog no. 781075) were employed. PTP1B (1−405 AA) and TC-PTP (2−345AA) were produced in house (Boehringer-Ingelheim Pharma GmbH & Co. KG). The substrates for PTP1B and TC-PTP EDT-pY-Y-RKG-amide and biotin-Ahx-EDT-pY-Y-RKG-amide were purchased from Biosyntan (Berlin, Germany), whereas pFYN for the PTP1B pFYN assay was purchased from Biotrend (Köln, Germany, catalog no. 435305). Anti-phosphotyrosine antibody clone 4G10 was purchased at Merck Millipore (Darmstadt, Germany, catalog no. 05-321). Orthovanadate was bought at Biolabs (Ipswhich, USA, catalog no. P0758). The AlphaScreen IgG detection kit was obtained from PerkinElmer (Rodgau, Germany, catalog no. 6760617R). All other materials were of highest grade commercially available.

An amount of 100 nL of a test compound in various concentrations up to 500 μM was added into a microtiter plate, followed by the addition of 5 μL of a phosphatase (final concentration 500 pM). After an incubation time of 10 min at 24 °C 5 μL of the EDT-pY-Y-RKG-amide substrate (final concentration of 1.4 μM) or pFYN substrate (final concentration of 20 μM) were added. Plates were then incubated in a humidified incubator at 24 °C for 1.5 h. To stop the enzymatic reaction, 5 μL of orthovanadate (final concentration 200 μM) was added. Each microtiter plate contained low controls (buffer instead of enzyme) and high controls (enzyme). Furthermore, each microtiter plate contained a standard curve using EDT-pY-Y-RKG-amide in the concentration range 30 μM/3 μM/1 μM/300 nM/100 nM/30 nM/10 nM/1 nM or pFYN in the range of 300 μM/100 μM/30 μM/3 μM/1 μM/300 nM/100 nM/30 nM.

5 μL of biotin-Ahx-EDT-pY-Y-RKG-amide and streptavidin donor bead mix (final concentration of 2.5 nM substrate and 5 μg/mL donor beads) were added, followed by the addition of 5 μL acceptor bead and antibody mix (final concentration of 5 μg/mL acceptor bead and 500 pM antibody). After an incubation time of 2 h at 24 °C the AlphaScreen signal was measured with an Envision reader (PerkinElmer). Data were analyzed by using the standard curve on each plate.

Computational Methods. *Protein Preparation.* hSTEP PTP domain X-ray structure bound to **2** was superposed with PDB code 2BV5 to model the missing loop (manual transfer) and the acetylation of the active site Cys496 was removed. **2** was replaced by BI-0314 by superposing mouse and human STEP structures. The resulting structure was treated by the protein preparation procedure including protonation by protonate3D as implemented in MOE,[42] and a stepwise energy minimization was done employing the MMFF94x force field (position restraints 0.0, 1.0 on heavy atoms, followed by 1.0 on the backbone). The protonation state of the active site cysteine Cys496 was manually adjusted.

MD Simulations. Molecular dynamics simulations were carried out using the AMBER 14 package[43] employing the ff14SB force field and the TIP3P water model. The AM1-BCC method was used to obtain partial charges for the ligands with the antechamber tool. A truncated octahedral solvation bounding box of 90 Å and periodic boundary conditions with the Ewald approach were employed. Equilibration of the system was done by a stepwise schedule, starting with heating from 100 to 300 K in the *NVT* ensemble, transitioning to the *NPT* ensemble at 300 K with stepwise lowering of the constraints on the protein heavy atoms. For the production runs 40 MD simulations of apo STEP and 60 runs of BI-0314 bound STEP (each 100 ns), employing a time step of 2 fs with the SHAKE algorithm, were performed. 44 trajectories of BI-0314 bound STEP qualified for further analysis because the ligand rmsd was <3.5 Å throughout the MD, corresponding to proper binding. The simulations were repeated with deprotonated Cys496, resulting in basically identical results for the *B*-factor analysis. Twenty trajectories each, from the apo simulation and from the liganded simulations, were subjected to the Allosteer[30] analysis to identify the allosteric pathways.

■ ASSOCIATED CONTENT

Supporting Information

The Supporting Information is available free of charge on the ACS Publications website at DOI: 10.1021/acs.jmedchem.8b00857.

^{15}N TROSY NMR spectra of **2** with human and mouse STEP PTP; crystal contacts in mouse and human STEP close to the allosteric binding site; ^{15}N TROSY NMR spectrum of BI-0314 on human STEP and determination of the KD; ITC measurements of the binding affinity of BI-0314 toward hSTEP; activation of mouse STEP PTP domain by BI-0314; enzyme progress curves for human STEP PTP domain; allosteric binding sites and allosteric pipelines; comparison of mSTEP, apo vs bound to BI-0314; calculated *B*-factors upon binding of BI-0314; DSF spectrum of BI-0314 binding to human STEP; allosteric pipelines and comparison to PTP1B; X-ray statistics; NMR chemical shift perturbation; other comments on hit finding; compound characterization; ^{1}H NMR of BI-0314; ^{13}C NMR of BI-0314 (PDF)

Molecular formula strings (CSV)

Accession Codes

Atomic coordinates of human STEP in complex with **2** (PDB code 6H8R) and of mouse STEP in complex with BI-0314 (PDB code 6H8S) have been deposited with the Protein Data Bank.

■ AUTHOR INFORMATION

Corresponding Author

*E-mail: christofer.tautermann@boehringer-ingelheim.com.

ORCID

Christofer S. Tautermann: 0000-0002-6935-6940

Nagarajan Vaidehi: 0000-0001-8100-8132

Notes

The authors declare no competing financial interest.

■ ACKNOWLEDGMENTS

We thank Anita Bloching, Heidi Bosch, Jessica Bretzel, Julian Friedl, and Franziska Moser for excellent technical assistance; Stephanie Merkle, Katja Philipp, and Achim Bixenmann for compound syntheses; Kathrin Feuerstein for compound analytics; Dominik Frey and Achim Lietz for compound profiling (biochemical assays); and Markus Holstein for setting up and performing RapidFire MS/MS analytics.

■ ABBREVIATIONS USED

PTPN5, protein tyrosine phosphatase non-receptor type 5; STEP, striatal-enriched protein tyrosine phosphatase; NMDAR, *N*-methyl-D-aspartate receptor; AMPAR, α-amino-3-hydroxy-5-methyl-4-isoxazolepropionic acid receptor; AD, Alzheimer's disease; KIM, kinase interaction motif; PTP, protein tyrosine phosphatase; STD NMR, saturation transfer difference NMR; DSF, differential scanning fluorometry; MST, microscale thermophoresis; CSP, chemical shift perturbation; ITC, isothermal titration calorimetry

DOI: 10.1021/acs.jmedchem.8b00857
J. Med. Chem. XXXX, XXX, XXX−XXX

REFERENCES

(1) Goebel-Goody, S. M.; Baum, M.; Paspalas, C. D.; Fernandez, S. M.; Carty, N. C.; Kurup, P.; Lombroso, P. J. Therapeutic Implications for Striatal-Enriched Protein Tyrosine Phosphatase (STEP) in Neuropsychiatric Disorders. *Pharmacol. Rev.* **2012**, *64*, 65−87.

(2) Kurup, P.; Zhang, Y.; Xu, J.; Venkitaramani, D. V.; Haroutunian, V.; Greengard, P.; Nairn, A. C.; Lombroso, P. J. Aβ-Mediated NMDA Receptor Endocytosis in Alzheimer's Disease Involves Ubiquitination of the Tyrosine Phosphatase STEP61. *J. Neurosci.* **2010**, *30*, 5948−5957.

(3) Zhang, Y.; Kurup, P.; Xu, J.; Carty, N.; Fernandez, S. M.; Nygaard, H. B.; Pittenger, C.; Greengard, P.; Strittmatter, S. M.; Nairn, A. C.; Lombroso, P. J. Genetic Reduction of Striatal-Enriched Tyrosine Phosphatase (STEP) Reverses Cognitive and Cellular Deficits in an Alzheimer's Disease Mouse Model. *Proc. Natl. Acad. Sci. U. S. A.* **2010**, *107*, 19014−19019.

(4) Kurup, P. K.; Xu, J.; Videira, R. A.; Ononenyi, C.; Baltazar, G.; Lombroso, P. J.; Nairn, A. C. STEP61 is a Substrate of the E3 Ligase Parkin and is Upregulated in Parkinson's Disease. *Proc. Natl. Acad. Sci. U. S. A.* **2015**, *112*, 1202−1207.

(5) Carty, N. C.; Xu, J.; Kurup, P.; Brouillette, J.; Goebel-Goody, S. M.; Austin, D. R.; Yuan, P.; Chen, G.; Correa, P. R.; Haroutunian, V.; Pittenger, C.; Lombroso, P. J. The Tyrosine Phosphatase STEP: Implications in Schizophrenia and the Molecular Mechanism Underlying Antipsychotic Medications. *Transl. Psychiatry* **2012**, *2*, e137.

(6) Goebel-Goody, S. M.; Wilson-Wallis, E. D.; Royston, S.; Tagliatela, S. M.; Naegele, J. R.; Lombroso, P. J. Genetic Manipulation of STEP Reverses Behavioral Abnormalities in a Fragile X Syndrome Mouse Model. *Genes, Brain and Behavior* **2012**, *11*, 586−600.

(7) Reinhart, V. L.; Nguyen, T.; Gerwien, R.; Kuhn, M.; Yates, P. D.; Lanz, T. A. Downstream Effects of Striatal-Enriched Protein Tyrosine Phosphatase Reduction on RNA Expression in Vivo and in Vitro. *Neuroscience* **2014**, *278*, 62−69.

(8) Xu, J.; Chatterjee, M.; Baguley, T. D.; Brouillette, J.; Kurup, P.; Ghosh, D.; Kanyo, J.; Zhang, Y.; Seyb, K.; Ononenyi, C.; Foscue, E.; Anderson, G. M.; Gresack, J.; Cuny, G. D.; Glicksman, M. A.; Greengard, P.; Lam, T. T.; Tautz, L.; Nairn, A. C.; Ellman, J. A.; Lombroso, P. J. Inhibitor of the Tyrosine Phosphatase STEP Reverses Cognitive Deficits in a Mouse Model of Alzheimer's Disease. *PLoS Biol.* **2014**, *12*, e1001923.

(9) Venkitaramani, D. V.; Moura, P. J.; Picciotto, M. R.; Lombroso, P. J. Striatal-Enriched Protein Tyrosine Phosphatase (STEP) Knockout Mice Have Enhanced Hippocampal Memory. *European Journal of Neuroscience* **2011**, *33*, 2288−2298.

(10) Zhang, Y.; Kurup, P.; Xu, J.; Anderson, G. M.; Greengard, P.; Nairn, A. C.; Lombroso, P. J. Reduced Levels of the Tyrosine Phosphatase STEP Block Beta Amyloid-Mediated GluA1/GluA2 Receptor Internalization. *J. Neurochem.* **2011**, *119*, 664−672.

(11) Olausson, P.; Venkitaramani, D. V.; Moran, T. D.; Salter, M. W.; Taylor, J. R.; Lombroso, P. J. The Tyrosine Phosphatase STEP Constrains Amygdala-Dependent Memory Formation and Neuroplasticity. *Neuroscience* **2012**, *225*, 1−8.

(12) Xu, J.; Kurup, P.; Baguley, T. D.; Foscue, E.; Ellman, J. A.; Nairn, A. C.; Lombroso, P. J. Inhibition of the Tyrosine Phosphatase STEP61 Restores BDNF Expression and Reverses Motor and Cognitive Deficits in Phencyclidine-Treated Mice. *Cell. Mol. Life Sci.* **2016**, *73*, 1503−1514.

(13) Kulikova, E. A.; Volcho, K. P.; Salakhutdinov, N. F.; Kulikov, A. V. Benzopentathiepine Derivative, 8-(Trifluoromethyl)-1,2,3,4,5-Benzopentathiepin-6-Amine Hydrochloride (TC-2153), as a Promising Antidepressant of New Generation. *Lett. Drug Des. Discovery* **2017**, *14*, 974−984.

(14) Witten, M. R.; Wissler, L.; Snow, M.; Geschwindner, S.; Read, J. A.; Brandon, N. J.; Nairn, A. C.; Lombroso, P. J.; Käck, H.; Ellman, J. A. X-Ray Characterization and Structure-Based Optimization of Striatal-Enriched Protein Tyrosine Phosphatase Inhibitors. *J. Med. Chem.* **2017**, *60*, 9299−9319.

(15) Rankovic, Z. Cns Drug Design: Balancing Physicochemical Properties for Optimal Brain Exposure. *J. Med. Chem.* **2015**, *58*, 2584−2608.

(16) He, R.; Zeng, L.-F.; He, Y.; Zhang, S.; Zhang, Z.-Y. Small Molecule Tools for Functional Interrogation of Protein Tyrosine Phosphatases. *FEBS J.* **2013**, *280*, 731−750.

(17) Chen, Y.-N. P.; LaMarche, M. J.; Chan, H. M.; Fekkes, P.; Garcia-Fortanet, J.; Acker, M. G.; Antonakos, B.; Chen, C. H.-T.; Chen, Z.; Cooke, V. G.; Dobson, J. R.; Deng, Z.; Fei, F.; Firestone, B.; Fodor, M.; Fridrich, C.; Gao, H.; Grunenfelder, D.; Hao, H.-X.; Jacob, J.; Ho, S.; Hsiao, K.; Kang, Z. B.; Karki, R.; Kato, M.; Larrow, J.; La Bonte, L. R.; Lenoir, F.; Liu, G.; Liu, S.; Majumdar, D.; Meyer, M. J.; Palermo, M.; Perez, L.; Pu, M.; Price, E.; Quinn, C.; Shakya, S.; Shultz, M. D.; Slisz, J.; Venkatesan, K.; Wang, P.; Warmuth, M.; Williams, S.; Yang, G.; Yuan, J.; Zhang, J.-H.; Zhu, P.; Ramsey, T.; Keen, N. J.; Sellers, W. R.; Stams, T.; Fortin, P. D. Allosteric Inhibition of SHP2 Phosphatase Inhibits Cancers Driven by Receptor Tyrosine Kinases. *Nature* **2016**, *535*, 148.

(18) Krishnan, N.; Koveal, D.; Miller, D. H.; Xue, B.; Akshinthala, S. D.; Kragelj, J.; Jensen, M. R.; Gauss, C.-M.; Page, R.; Blackledge, M.; Muthuswamy, S. K.; Peti, W.; Tonks, N. K. Targeting the Disordered C Terminus of PTP1B with an Allosteric Inhibitor. *Nat. Chem. Biol.* **2014**, *10*, 558−566.

(19) Wiesmann, C.; Barr, K. J.; Kung, J.; Zhu, J.; Erlanson, D. A.; Shen, W.; Fahr, B. J.; Zhong, M.; Taylor, L.; Randal, M.; McDowell, R. S.; Hansen, S. K. Allosteric Inhibition of Protein Tyrosine Phosphatase 1B. *Nat. Struct. Mol. Biol.* **2004**, *11*, 730−737.

(20) Sharma, E.; Zhao, F.; Bult, A.; Lombroso, P. J. Identification of Two Alternatively Spliced Transcripts of Step: A Subfamily of Brain-Enriched Protein Tyrosine Phosphatases. *Mol. Brain Res.* **1995**, *32*, 87−93.

(21) Li, R.; Xie, D.-D.; Dong, J.-h.; Li, H.; Li, K.-s.; Su, J.; Chen, L.-Z.; Xu, Y.-F.; Wang, H.-M.; Gong, Z.; Cui, G.-Y.; Yu, X.; Wang, K.; Yao, W.; Xin, T.; Li, M.-Y.; Xiao, K.-H.; An, X.-f.; Huo, Y.; Xu, Z.-g.; Sun, J.-P.; Pang, Q. Molecular Mechanism of ERK Dephosphorylation by Striatal-Enriched Protein Tyrosine Phosphatase. *J. Neurochem.* **2014**, *128*, 315−329.

(22) Barr, A. J.; Ugochukwu, E.; Lee, W. H.; King, O. N. F.; Filippakopoulos, P.; Alfano, I.; Savitsky, P.; Burgess-Brown, N. A.; Müller, S.; Knapp, S. Large-Scale Structural Analysis of the Classical Human Protein Tyrosine Phosphatome. *Cell* **2009**, *136*, 352−363.

(23) Erlanson, D. A.; Fesik, S. W.; Hubbard, R. E.; Jahnke, W.; Jhoti, H. Twenty Years On: The Impact of Fragments on Drug Discovery. *Nat. Rev. Drug Discovery* **2016**, *15*, 605−619.

(24) Jahnke, W.; Rondeau, J.-M.; Cotesta, S.; Marzinzik, A.; Pellé, X.; Geiser, M.; Strauss, A.; Götte, M.; Bitsch, F.; Hemmig, R.; Henry, C.; Lehmann, S.; Glickman, J. F.; Roddy, T. P.; Stout, S. J.; Green, J. R. Allosteric Non-Bisphosphonate FPPS Inhibitors Identified by Fragment-Based Discovery. *Nat. Chem. Biol.* **2010**, *6*, 660−666.

(25) Cox, A. D.; Fesik, S. W.; Kimmelman, A. C.; Luo, J.; Der, C. J. Drugging the Undruggable RAS: Mission Possible? *Nat. Rev. Drug Discovery* **2014**, *13*, 828−851.

(26) Eswaran, J.; von Kries, J. P.; Marsden, B.; Longman, E.; Debreczeni, J. É.; Ugochukwu, E.; Turnbull, A.; Lee, W. H.; Knapp, S.; Barr, A. J. Crystal Structures and Inhibitor Identification for PTPN5, PTPRR and PTPN7: A Family of Human MAPK-Specific Protein Tyrosine Phosphatases. *Biochem. J.* **2006**, *395*, 483−491.

(27) Francis, D. M.; Page, R.; Peti, W. Sequence-Specific Backbone 1H, 13C and 15N Assignments of the 34 kDa Catalytic Domain of PTPN5 (STEP). *Biomol. NMR Assignments* **2014**, *8*, 185−188.

(28) Klebe, G. Applying Thermodynamic Profiling in Lead Finding and Optimization. *Nat. Rev. Drug Discovery* **2015**, *14*, 95−110.

(29) Welte, S.; Baringhaus, K.-H.; Schmider, W.; Müller, G.; Petry, S.; Tennagels, N. 6,8-Difluoro-4-Methylumbiliferyl Phosphate: A Fluorogenic Substrate for Protein Tyrosine Phosphatases. *Anal. Biochem.* **2005**, *338*, 32−38.

(30) Bhattacharya, S.; Vaidehi, N. Differences in Allosteric Communication Pipelines in the Inactive and Active States of a GPCR. *Biophys. J.* **2014**, *107*, 422−434.

DOI: 10.1021/acs.jmedchem.8b00857
J. Med. Chem. XXXX, XXX, XXX−XXX

(31) Brandão, T. A. S.; Hengge, A. C.; Johnson, S. J. Insights into the Reaction of Protein-Tyrosine Phosphatase 1B: Crystal Structures for Transition State Analogs of Both Catalytic Steps. *J. Biol. Chem.* **2010**, *285*, 15874−15883.
(32) Choy, M. S.; Li, Y.; Machado, L. E. S. F.; Kunze, M. B. A.; Connors, C. R.; Wei, X.; Lindorff-Larsen, K.; Page, R.; Peti, W. Conformational Rigidity and Protein Dynamics at Distinct Timescales Regulate PTP1B Activity and Allostery. *Mol. Cell* **2017**, *65*, 644−658.
(33) Lipchock, J. M.; Hendrickson, H. P.; Douglas, B. B.; Bird, K. E.; Ginther, P. S.; Rivalta, I.; Ten, N. S.; Batista, V. S.; Loria, J. P. Characterization of Protein Tyrosine Phosphatase 1B Inhibition by Chlorogenic Acid and Cichoric Acid. *Biochemistry* **2017**, *56*, 96−106.
(34) Mayer, M.; Meyer, B. Characterization of Ligand Binding by Saturation Transfer Difference NMR Spectroscopy. *Angew. Chem., Int. Ed.* **1999**, *38*, 1784−1788.
(35) Ross, A.; Senn, H. Automation of Biomolecular NMR Screening. *Curr. Top. Med. Chem.* **2003**, *3*, 55−67.
(36) Pervushin, K. V.; Wider, G.; Wüthrich, K. Single Transition-to-Single Transition Polarization Transfer (ST2-PT) in [15N,1H]-TROSY. *J. Biomol. NMR* **1998**, *12*, 345−348.
(37) Vonrhein, C.; Flensburg, C.; Keller, P.; Sharff, A.; Smart, O.; Paciorek, W.; Womack, T.; Bricogne, G. Data Processing and Analysis with the Autoproc Toolbox. *Acta Crystallogr., Sect. D: Biol. Crystallogr.* **2011**, *67*, 293−302.
(38) Collaborative Computational Project, Number 4.. The CCP4 Suite: Programs for Protein Crystallography. *Acta Crystallogr., Sect. D: Biol. Crystallogr.* **1994**, *50*, 760−763.
(39) Emsley, P.; Lohkamp, B.; Scott, W. G.; Cowtan, K. Features and Development of Coot. *Acta Crystallogr., Sect. D: Biol. Crystallogr.* **2010**, *66*, 486−501.
(40) Bricogne, G.; Blanc, E.; Brandl, M.; Flensburg, C.; Keller, P.; Paciorek, W.; Roversi, P.; Sharff, A.; Smart, O. S.; Vonrhein, C.; Womack, T. O. *Buster*, version 2.11.2; Global Phasing Ltd., 2017.
(41) Chen, V. B.; Arendall, W. B., III; Headd, J. J.; Keedy, D. A.; Immormino, R. M.; Kapral, G. J.; Murray, L. W.; Richardson, J. S.; Richardson, D. C. Molprobity: All-Atom Structure Validation for Macromolecular Crystallography. *Acta Crystallogr., Sect. D: Biol. Crystallogr.* **2010**, *66*, 12−21.
(42) *Molecular Operating Environment (MOE)*, version 2016.08; Chemical Computing Group, 2017.
(43) Case, D. A.; Babin, V.; Berryman, J. T.; Betz, R. M.; Cai, Q.; Cerutti, D. S.; Cheatham, T. E.; Darden, T. A.; Duke, R. E.; Gohlke, H.; Goetz, A. W.; Gusarov, S.; Homeyer, N.; Janowski, P.; Kaus, J.; Kolossváry, I.; Kovalenko, A.; Lee, T. S.; LeGrand, S.; Luchko, T.; Luo, R.; Madej, B.; Merz, K. M.; Paesani, F.; Roe, D. R.; Roitberg, A.; Sagui, C.; Salomon-Ferrer, R.; Seabra, G.; Simmerling, C. L.; Smith, W.; Swails, J.; Walker, R. C.; Wang, J.; Wolf, R. M.; Wu, X.; Kollman, P. A. *AMBER 14*; University of California, San Francisco, 2014.

DOI: 10.1021/acs.jmedchem.8b00857
J. Med. Chem. XXXX, XXX, XXX−XXX